Heterogeneous acid catalyst preparation from olive pomace and its use for olive pomace oil esterification

Manel Ayadi, Sary Awad, Audrey Villot, Manef Abderrabba, Mohand Tazerout

Heterogeneous Acid Catalyst Preparation from Olive Pomace and its Use for Olive Pomace Oil Esterification

Manel AYADI [a,b], Sary AWAD[a,*], Audrey VILLOT[a], Manef ABDERRABBA[b], Mohand TAZEROUT[a]

a: department of Energy Systems and Environment (DSEE), IMT Atlantique

b: Laboratory of Materials, Molecules and Applications, University of Carthage, IPEST La Marsa Tunisia, Faculty of Sciences of Bizerte

*** corresponding author :** Sary AWAD, Energy Systems and Environment Department (DSEE), IMT Atlantique, 4 rue Alfred Kastler, 44307, Nantes, France. **E-mail**: sary.awad@gmail.com, **Tel:** +33 2 51 85 85 61

Abstract:

Solid acid catalyst was produced from olive pomace (OP), characterized and used for the esterification of OP oil. OP was pyrolyzed, physical activated by steam and sulfonated using sulfuric acid. Commercial, coconut husk-based, activated carbon (CHAC) was also sulfonated for comparison. The activation has shown a significant increase in olive pomace activated carbon (OPAC) surface area by developing simultaneously its micro and meso-porosity. The sulfonation has further increased OPAC BET surface area to reach 618.18 m²/g and has changed its structure to become microporous. Sulfonation also removed tar residues and aliphatic hydrocarbons from OPAC's surface. Tendencies observed with carbon CHAC, used for comparison, are slightly different with a mesoporosity development. Although its higher surface area (1227.01 m²/g), CHAC has fixed three times less sulfur than OPAC, which can be attributed to its higher hydrophobicity or pore distribution. Sulfur was mainly fixed in the form of sulfonic acid (SO_3H). Esterification with methanol using produced solid catalysts decreased OPO acidity below the 2 mg_{KOH}/g threshold after 5 h of reaction and reduced mono, di and triglycerides to levels close to the ones required by European norm EN14214.

24 *Keywords:* Acid oil; biochar; esterification; olive pomace; solid acid catalyst;

25

Nomenclature

Abbreviations

AC	Activated carbon
AV	Acid value
CHAC	Coconut Husk Activated Carbon
CHACS	Sulfonated Coconut Husk Activated Carbon
FFA	Free Fatty Acids
OP	Olive Pomace
OPAC	Olive Pomace Activated Carbon
OPACS	Sulfonated Olive Pomace Activated Carbon
OPO	Olive Pomace Oil
TOF	Turn Over Frequency
TOF_{1h}	Turn Over Frequency after 1 h of reaction
TOF_{5h}	Turn Over Frequency after 5 h of reaction

Variables

C_s	Molar fraction of specie *s* (%)
C_{N2}	Molar fraction of N_2 (%)
k	Irreversible reaction rate constant (h^{-1})
k_1	Direct reaction rate constant (h^{-1})
k_2	reverse reaction rate constant (h^{-1})
M	Methanol concentration ($mol.l^{-1}$)
ME	Methyl ester concentration ($mol.l^{-1}$)
m_s	Mass of specie *s* (g)
M_s	Molar mass of specie *s* ($g.mol^{-1}$)
Q_{N2}	Nitrogen flowrate (l/min)
V_s	Molar volume of specie *s* ($l.mol^{-1}$)
W	Water concentration ($mol.l^{-1}$)

1- Introduction:

Tunisia is ranked second in the world in the production of olive oil with a number of trees exceeding 86 million. Oil represents only 20% of olives mass, the remaining fraction exits oil production process in forms of solid and liquid wastes (30% and 50% respectively) [1].

Olive pomace (OP), the solid by-product of olive oil, contains pieces of pit (42–54%), about 10–11% skin, and between 21 and 33% of pulp [2] and has an oil content that could reach 8% depending on extraction technology [2].

OP has a negative impact on the environment due to slightly acidic pH values, a high moisture content and a very high content of organic matter (lignin, hemicellulose and cellulose). Olive pomace is non-biodegradable due to its significant contents of water-soluble phenolic substances. Besides that, olive pomace contains water-soluble fats, proteins, water-soluble carbohydrates and it is rich in potassium and poor in phosphorus and micronutrients [3]. Olive pomace composition attributes it phytotoxic and antimicrobial properties [4]. Since OP is still rich in oil and polyphenol, it increases soil hydrophobicity and infiltration rate and decreases water retention rate in case of land spreading [5]. These environmental problems could be eliminated if the olive residue is either treated to extract olive pomace oil residue or used to obtain fuel [6]. However, this step increases process costs, and resolves partially the problem, because exhausted OP and extracted oil are still wastes that need to be treated. However, the valorization of these wastes into biosourced-materials and/or energy carriers, could enhance the economy of the process. For example, exhausted olive pomace can be used to produce activated carbon, while olive pomace oil (OPO) can be used for biodiesel production. However, OPO has a very high content of free fatty acids (FFA) which requires the use of acid catalysis followed by alkali catalysis. Among different types of catalysts, heterogeneous ones are preferable

because of their lower corrosiveness, their reusability and for the ease of separation during process.

Several studies have been led on the use of sulfonated char and activated carbon as solid catalysts for esterification of FFA because of sustainability and integrability in processes. In fact, these materials are byproducts of biorefineries and their use reduces the need for metal catalysts and fossil fuel derived ones [7]. Furthermore, these catalysts present the advantage of having very high specific surface area ranging from 200 to 1500 m^2/g besides their non-polarity that prevents them from being deactivated because of water and/or glycerol produced during esterification and/or transesterification reactions [8]. In fact, hydrophilic structures, adsorbs water generated during esterification reaction which deactivates acid sites [9].

Carbon based catalysts can be obtained by simply impregnating char/activated carbon with sulfuric acid [10] or by exposing it to SO_3 [8] in order to functionalize the surface with sulfonic acid (SO_3H).

Extensive research on sulfonated AC conducted by Dehkhoda et al [11] prove that the more powerful the use of the sulfonating agent, the higher the acid density in the catalysts is produced. These results are in agreement with the results of Kastner et al. who made a comparative study between sulfonated AC prepared from biochar and wood-based materials. They examined the catalytic activity of catalysts during the esterification of fatty acids. According to their work the sulfonated AC catalyst made from wood is more efficient because of its higher activity. However, catalyst reuse was not possible due to water absorption and -SO_3H leaching, which leads to a decrease in its specific surface area and a reduction in acid density similar to other sulfonated AC [8].

The aim of the present work is to investigate the production of a solid acid catalyst from olive pomace by pyrolysis/activation followed by a sulfonation using sulfuric acid. To the knowledge

of the authors this cheap and highly available raw material is not well explored in literature. There are few works that dealt with the production and characterization of biochar and on its use as an adsorbent [3]. No works were found in literature about AC production from olive pomace neither on its use as a catalyst for esterification. The originality of the present work resides in the suggestion of an integrated solution for the production of AC and biodiesel from olive oil by-products. The produced solid catalyst can compete at the same time with homogeneous catalysts and with Commercial, coconut husk activated carbon -based solid catalyst.

2- Materials and methods

2.1. Raw materials and chemicals

Olive pomace and olive pomace oil used in this study were supplied by Abou El-Walid Company located in Tunisia. In this company, hexane extraction is used to recover pomace oil. This oil has a high content of FFA reaching 60 wt.%. The remaining are mono, di and triglycerides (glycerides) and it has a kinematic viscosity of 26.8 mm^2/s at 40°C. FFA are mainly composed of oleic Acid (57%), palmitic acid (16.5%), linoleic acid (15.7%)and stearic acid (4%). Its mean molecular weight is 292 g/mol.

Commercial, coconut husk based activated carbon, (CHAC) used in this work for comparison was furnished by Jacobi Carbons France (PICA).

Methanol having 98% purity and 17 M sulfuric acid were purchased from Sigma-Aldrich

2.2. Olive Pomace and Olive Pomace Oil characterization

2.2.1 Chemical analysis:

Olive pomace was dried and grinded (by RETSCH MM400 scale series laboratory mill) and sieved to powder of sizes < 1 mm. The organic composition of raw materials, CHNS and O, was measured by A Thermofinnigan EA 1112 elemental analyzer (Thermo-finnigane instrument). Same procedure was also applied for biochar, activated carbons and catalysts elemental analysis. The inorganic composition of raw materials was analyzed by X-ray fluorescence spectrometry (SHIMADZU EDX-500HS) which is a semi-quantitative method. The error percentage of this analysis is considered to be around 20% for the main elements in ash composition.

2.2.2. TGA analysis

The proximate analysis was carried out using a SETSYS Evolution Thermogravimetric Analyzer (TGA) following the ASTM standards: ASTM D3175 [12] for volatile matter. TGA was also used to determine the lignocellulosic material content distribution, for that the olive pomace materials were heated under an inert gas flow to a final temperature of 900 °C with a heating rate of 10 °C.min^{-1}, with intermediate plateaus at 100°C, 250 °C, 350 °C and 500 °C corresponding to the evaporation of moisture and the final degradation temperatures of hemicellulose, cellulose and lignin respectively [13].

To conduct the analysis, protective gas, argon, is passed through the thermobalance to protect it from possible corrosive gases. The process was carried out on samples weighing between 3 mg – 10 mg. a flow of nitrogen of 100 cm^3.min^{-1} was used to ensure an inert condition and the removal of the pyrolytic gases.

2.2.3. Ash content of olive pomace and carbonaceous supports

The ash content of different products was determined by placing dry samples in a laboratory muffle furnace (Nabertherm p330) Following the ASTM D1102 [14] for ash content of the biomass and ASTM D3174 [15] for ash content of the char.

2.2.4. Determination of olive pomace oil (and methyl esters) acid value:

The acid value is determined by titration of the oil (before and after esterification) using a standardized titration solution of KOH in ethanol, according to the ASTM D664 method [16].

2.3. Preparation of heterogeneous catalyst

2.3.1. Preparation of pyrolysis char and activated carbon

Olive pomace is pyrolyzed up to 800°C with a heating rate of 10°C/min under nitrogen flow using setup presented in fig 1. For that, 400 g of olive pomace were introduced in a semi-rotating quartz tube under N_2 flow of 0.75 SLPM (standard liters per minute measured at 100 kPa and 0°C). At the end of this step, it is possible to cool-down the system at room temperature. The raw char, denoted hereafter as Biochar, and the condensable phase can be collected and weighted. The condensable gases (steam and light tars) were removed by a cold trap close to 0 °C and the gases analyzed by the GC. The pyrolysis gas was analyzed by online gas micro-chromatography (SRA Instruments R 3000) equipped with a thermal conductivity detector. This technique was able to measure the non-condensable gases such as H_2, O_2, N_2, CH_4, CO, CO_2, C_2H_4, C_2H_6, C_3H_8 and C_3H_6. The system performed a complete analysis every 3 min, and the mass of each gaseous specie (m_s) was evaluated by the expression given in equation 1 [19]:

$$m_s = M_S \frac{Q_{N2}}{V_m} \int_{t_0}^{t_f} \frac{C_S}{C_{N2}} dt \quad (1)$$

where the interval of integration corresponds to the elapsing time of analysis, C_S represents the molar fraction of the detected species and M_s its molecular weight, Q_{N2} is the nitrogen flow rate and C_{N2} the nitrogen molar fraction, and V_m is the molar volume. The pyrolysis was repeated at least 3 times and the average biochar yield was close to 30.8± 0.3%.

In order to produce activated carbon, superheated steam was used in order to increase the specific surface area of the biochar and increase its microporosity. When the temperature of 800°C is reached, the nitrogen atmosphere is switched to a nitrogen/steam mixture (0.53 SLPM / 88 vol. % of N_2 and 0.7 mL.min^{-1} of H_2O / 12 vol. %). The activated chars were denoted as OPAC.

2.3.2. Sulfonation of biochar and activated carbon:

Biochar, OPAC and CHAC are sulfonated using 17 M Sulfuric acid, under vigorous stirring during 15 min. Excess acid was eliminated by decantation and solid residue was poured into a ceramic crucible and introduced to muffle furnace preheated to 100°C and kept during 18 h. Finally, sulfonated material was profusely washed with distilled water before being dried in oven at 105°C overnight. Washing step was performed in order to ensure that the remaining SO_3H sites are highly stable. Washing consisted on several soaking and pouring, through a sieve, steps with distilled water until the water leaving sieve is neutral. Then catalyst was soaked in water, stirred for 2 h, then left overnight before pouring water and verifying its pH stability.

As per sulfuric acid/OP ratio. The ratio was optimized by impregnating different amounts of sulfuric acid on OPAC and by realizing an acid esterification for 1 h of OP. Optimization started by using the amount suggested by Kastner et al. [8] and it was each time divided by 2 until noticing a significant decrease in catalytic activity. The optimal amount that was found is 0.4 g_{H2SO4}/g_{AC} and it was adopted for the sulfonation of different carbonaceous materials used in this study.

2.4 Biochar, Activated carbon and Catalyst analysis:

2.4.1 BET surface and porosity analysis

The specific surface area was determined using the Brunauer-Emmet-Tellet (BET) method under nitrogen adsorption/desorption isotherms of nitrogen at - 196 °C (Micromeritics ASAP 2020). This model is based on the principle of formation of multilayers but only the first layer of adsorbate molecules is attached to the solid surface by adsorbent-adsorbate adsorption forces. Currently BET model is the most applied to determine surface areas thus it can be taken as a reference method [20]. The Barrett-Joyner Halenda (BJH) and Horvath Kawazoe methods were respectively used to characterize the microporosity (pore diameters < 2 nm) and the mesoporosity (2 < pore diameters < 50 nm) [21].

2.4.2. X-ray diffraction analysis (XRD):

XRD is usually used to determine the patterns existing in the structure of materials. Typically, it determines the crystallinity degree of a material and the type of crystalline structure. Furthermore, due to a large library of spectra it is also possible to determine the nature of stacks or clusters present in the material (aromatic, aliphatic, unsaturated …).

The XRD patterns were monitored by X ray diffraction ex-situ using the apparatus Siemens D-5000. It is focused by a Ge crystal primary monochromator of which Ni-filtered Cu Kα1 radiation, lambda = 1.54056 Å, with θ/ 2θ diffraction instrument operating in reflection geometry, and the tube of copper is run at 40 mA and 40 kV.

2.4.3. Fourier Transform Infrared Spectroscopy analysis (FT-IR):

FTIR spectroscopy was carried out in an ATR Bruker Tensor 27, model 2012. Spectra were recorded in the range 4000-400 cm^{-1}, 50 scans were taken at a 0.1 cm s^{-1} scan rate and 2 cm^{-1} resolution. This technique is used to determine the chemical functions and bonds present on the surface of analyzed materials. In this study it helps to determine the chemical bonds in which sulfur, that was fixed on the material, is involved. Furthermore, it could help to detect the

189 presence of other species present on the surface of activated carbon that could also play a role
190 in the catalysis of esterification reaction.

191 *2.4.4 Scanning Electron Microscopy (SEM):*

192 A scanning electron microscope SEM, **JEOL JSM 7600F, JEOL JSM 5800LV** equipped with
193 a SDD SAMx energy dispersion spectrometer and JEOL (hybrid of two microscopes), was used
194 to characterize the surface morphologies of carbonaceous materials.

195 *2.4.5. X-Ray Fluorescence spectrometry (XRF):*

196 Bulk chemical composition of different materials was determined with a "SHIMADZU" X-ray
197 fluorescence (XRF) analyzer fitted with an EDX 800 HS X-ray tube, a gas scintillation detector
198 and a PR-10 anode. Analyzed materials were dried, crushed and sieved before analysis. 0.5 g
199 samples were used each time. CHON analysis results were taken in consideration during XRF
200 results treatment.

201 *2.4.6. Micro-GC*

202 Gas chromatography is used to determine the molar (or volume) composition of gases produced
203 during pyrolysis and activation processes. The apparatus used is a G2801A Model 3000A
204 Micro GC gas chromatography (Agilent Technologies, China), having two independent
205 systems (A and B) each consisting of an injector, a column and a thermal conductivity detector
206 (TCD). Both systems use Argon as the carrier gas.

207 The detector of system A makes it possible to identify H_2, CH_4, CO and N_2. The system B
208 detector identifies CO_2, H_2O, C_2H_2, C_2H_4, C_2H_6, C_3H_6, C_3H_8, C_4H_6, C_4H_8 and C_4H_{10}.

209 *2.4.7. Hydrophobicity*

After drying the OPAC and CHAC samples, they are placed in a stainless steel support with a mesh size of 0.8 mm. These samples are swept by a dry air flow of 50 cm^3/min and by a stream of water vapor whose humidity is 50%. The measurement of the hydrophobicity was made at ambient temperature and atmospheric pressure. The parameters of the "dry airflow and water vapor flow" experiment are set using a humid air generator, "OMICRON Technologies", introduced into a reactor at a total flow of 15 cm^3/min, during 3 h. At the end of the humidification, OPAC and CHAC are weighed and put in the oven at 105 °C for 18h, and then they are reweighed to calculate the amount of absorbed moisture.

2.5. Pyrolysis and activation's gaseous products analysis

At the outlet of reactor, gas samples were collected and injected into a micro-GC for analyzer. Samples were taken during pyrolysis and activation at time intervals of 10 min in order to detect the following gases: H_2, CO, CO_2, CH_4 and light hydrocarbons (C_xH_y). An additional sample was taken 2 min after steam injection in order to highlight the shift between pyrolysis and activation. The molar composition of gases was set after subtracting the N_2 fraction.

2.6. Olive Pomace Oil Esterification

Olive pomace oil esterification was performed in a batch reactor at 60°C under vigorous stirring during 5 h. Heterogeneous catalysis was performed using different methanol to FFA molar ratios (3:1, 6:1 and 9:1) and different loads (10, 15 and 20 wt.%) of produced heterogeneous catalyst. Homogeneous catalysis was performed, for comparison, using 3.6 wt% of 17 M sulfuric acid and 3:1 methanol to FFA ratio. Turn Over Frequency (TOF) was calculated for homogeneous and heterogeneous catalysts under different conditions for comparison. TOF was calculated as follows (eq 2).

$$TOF(h^{-1}) = \frac{FFA_0 - FFA_t}{SO_3H.t} \quad (2)$$

233 Where FFA_0 and FFA_t (moles) are the amounts of free fatty acids at the beginning and at time t
234 of reaction. SO_3H (moles) is the number of moles of acid sites present in catalyst calculated
235 based on the elemental analysis of heterogeneous catalyst. For homogeneous catalyst the
236 number of moles of H^+ was used.

237 Reaction order and rate constant (k) were determined for different studied reactions using the
238 integral method in order to understand underpinned phenomena observed for different
239 conditions.

240 2.7. GC-FID/MS Analysis

241 Gas chromatography coupled to flame ionization detector and to mass spectrometer (GC-
242 FID/MS) was used in order to determine the contents of fatty acid methyl esters, mono, di, and
243 triglycerides in oil samples and on the products having the lowest acid values using ASTM
244 method D 6584 [16]. This analysis will shed lights on the effects of used catalyst on
245 transesterification also.

246 The used GC column is an open tubular one with 5% phenylpolydimethylsiloxane bonded and
247 cross linked phase internal coating. FID temperature was set to 380°C. The column, is 15 m
248 long, has an internal diameter of 0.32 mm and 0.1 µm film thickness. 3 mL/min of hydrogen
249 was used as carrier. Internal standards used are butantriol and tricapran that were injected in
250 ratios 1:1:1 with respect to analyzed sample. Derivatization was ensured using N-methyl-N-
251 trimethylsilyltrifluoracetamide (MSTFA). The mass spectrometer was set at an ionizing voltage
252 of 70 eV and a range of m/z 30–450 respectively.

253 2.8. Viscosity measurement

254 Viscosity is a good indicator on the conversion rate of glycerides [17] as the viscosity of methyl
255 esters is between 6 – 12 times lower than that of triglycerides [18]. Thus, it was applied on the

samples having the lowest acid value (AV) in order to compare them to raw oil and to check out the effects of catalyst on transesterification.

Dynamic viscosity was measured at 40°C using an AND vibro viscometer. Density was measured using a pycnometer M50T (850 – 900 g/l) with a precision of 1 g/l. then kinematic viscosity was obtained by dividing it by the density according to test method EN ISO 3104 [19].

3- Results and discussion:

3.1. Pyrolysis and activation of olive pomace

In order to understand the impact of the pyrolysis and activation processes on the solid phase, gaseous products composition (CO_2, CO, CH_4, H_2 and light hydrocarbons (C_xH_y)) was followed all along the processes. At the first stage of reaction, CO and CO_2 started to appear at 230°C reaching a peak production between 350 and 370 °C which can be attributed to dehydration and decarboxylation of cellulose and hemicellulose [22]. CH_4 peak occurring between 560 and 620°C indicates lignin degradation. With temperature increasing from 480 to 800 °C the production of H_2 started and increased significantly as temperature increased. H_2 is a result of severe cracking of intermediary products and char that continues to emit light volatiles at high temperature levels [23]. Degradation ends at 580°C, temperature at which CO, hydrocarbons and CH_4 start decaying. At 680°C severe cracking of char continues to emit light volatiles (tar present in its pores and on its surface) at high temperature levels. These reactions are accompanied by a drastic increase in H_2 and CxHy production following dehydrogenation (eq. 3) and carbonization (eq. 4) reactions. CO also increases due to these reactions added to the decomposition of CO_2 into CO at high temperatures [24].

$$pC_xH_yO_z \rightarrow qC_nH_mO_t + rH_2 + sCO \quad (3)$$

279 $C_nH_mO_t \rightarrow (n-t)C + tCO + \frac{m}{2}H_2$ (4)

280 During pyrolysis, the heteroatoms are removed as volatiles. These degradation reactions
281 introduce a rearrangement of the carbon atoms, which form stacks of polyaromatic graphite
282 layers. Graphite is a layered structure in which the graphene layers are formed by carbon atoms
283 bonded by σ and π bonds to three other neighboring carbon atoms.

284 At 800 °C (t = 80 min) superheated water steam is injected during 80 min which corresponds to
285 the activation step. As it can be noticed in fig 2, 2 min right after the beginning of steam
286 injection, methane has drastically decreased while sharp increases of hydrogen, carbon dioxide
287 and hydrocarbons have been noticed. These results are in accordance with reactions 5 and 6,
288 where the activation step releases H_2. Hydrogen started to decrease right after the peak and
289 started to stabilize after 20 min at 55%. Methane production also continues decreasing until
290 reaching a plateau of 1.7% after 30 min

291 $C + H_2O \leftrightarrow CO + H_2$ (5)

292 $C0 + H_2O \leftrightarrow CO_2 + H_2$ (6)

293 CO volume concentration slightly increases from 17% to 21% during the first 30 min after
294 steam injection before starting a linear decrease reaching 14% at steam cut-off. Carbon dioxide
295 increases drastically from 0% (2 min after steam injection) up to 28% at steam cut-off.

296 The trends of these curves reveals the following reactional scheme:

297 Right after steam injection dehydrogenation and carbonization reactions continue to occur and
298 water steam triggers water-gas reaction that involves solid carbon (eq 5) and steam methane
299 reforming (eq 7). That explains the sharpening of H_2 and CH_4 slopes

300 $CH_4 + H_2O \leftrightarrow CO + H_2$ (7)

After 2 min of reaction, the available amount of tar present in the pores and on the surface of char starts to decrease, which leads to lower rates of reactions 3, 5 and 7 and to the decrease of curves slopes. At this stage, H_2 starts to decrease and CH_4 slope becomes less steep. At this moment water gas shift reaction (eq 6) is triggered where produced CO starts to oxidize into CO_2. This reaction is triggered due to the lack of methane that has a more affinity to water steam at these temperatures. After 30 min, when methane reforming decays, the trade-off between CO and CO_2 can be clearly noticed.

Among the up-listed reactions, water-gas and carbonization reactions affect the structure of activated carbon. The atmosphere of the oven containing H_2O makes it possible to develop cone-shaped pores, generated by carbon gasification reactions Eq.6. These observations are consistent with the results reported by Prauchner M. and Rodriguez-Reinoso F. [25] for activated carbon produced from coconut shells.

3.2 ***Characterization of olive pomace, biochar, activated carbon and catalysts***

3.2.1 Proximate and ultimate analysis:

The elemental compositions of olive pomace and carbonaceous materials are given in Table 1. Olive pomace has a high oxygen content reaching 41.51% of its weight. It contains 22.77% Cellulose, 19.8% Hemicellulose, 17.8% lignin, 21% fixed carbon and 0.32% Ash. The analysis results are comparable to those found elsewhere in literature [26]. Fixed carbon content of olive pomace makes it a good raw material for the preparation of activated carbon, because, it reflects the total carbon present in the final product [27].

After pyrolysis, oxygen content of bio-char has been reduced to 4.4 % due to decarboxylation and dehydration reactions. Hydrogen content was also reduced to 1.76% due to dehydration and depolymerization reactions. This evolution is explained by the breaking of the weakest chemical bonds (C-O, C-H) under the temperature effect [26]. According to the literature, the

increase of pyrolysis temperature increased the elimination of heteroatoms (O, H, N) in the form of volatile compounds is accentuated as well as the carbon content and the aromaticity of the char [29]. Nitrogen and oxygen that remain inside the char could be possibly embedded inside the biomass far from the surface. In fact, nitrogen and oxygen that leave out in form of volatile matter are most likely on the surface of feedstock where they can react with light free radicals before being swept out of the reactor. Nitrogen and oxygen inside the organic matter have more chances to recombine with carbon atoms and to integrate the solid carbon matrix. The pyrolysis allowed to limit the mineral species volatilization (an increase of ash rate), resulting in a highly concentrated carbon and mineral species in the matrix of the char.

Activation has further concentrated carbon by decreasing the content of all other components. Carbon content passed from 77.95% to 85% and oxygen, nitrogen and hydrogen have been decreased by half. Ash content has also slightly increased due to this step. OPAC has similar elemental composition to CHAC. Differences lie mainly in a lower carbon content of OPAC and a slightly higher ash and nitrogen contents.

The sulfonation of bio-char has not apparently succeeded. Sulfur content was lower than CHONS analyzer detection limits after sulfuric acid treatment. While carbon and hydrogen contents have decreased, nitrogen and oxygen contents have increased. A slight increase of ash content has been also detected. These observations indicate that sulfuric acid has mainly attacked the surface of bio-char and did not get deeper inside the material.

Sulfonation of OPAC and CHAC led to sulfur fixation that was accompanied by carbon contents decrease and oxygen increase by almost 5 folds for OPAC and 3 folds for CHAC. It was observed also that oxygen increase was proportional to sulfur fixation which could be explained by the fixation of $–SO_3H$ functional group on the surface of the catalyst [30].

3.2.2 BET analysis

The analysis of adsorption and desorption isotherms is done in order to get information about porous structure of activated carbon OPAC, CHAC, OPACS and CHACS. According to IUPAC classification, the N_2 adsorption-desorption isotherms of CHAC and CHACS, deemed to be type I, thus confirming the typical characteristics of porous activated carbon. OPAC and OPACS considered, deemed to be type IV, is typical for many ordered organic-inorganic nanocomposites with accessible mesopores although when the size of these pores is close to the micropore range or pore size distribution is broad, type I isotherms can be observed. This is also supported by the volume distribution between micro and mesoporous volume given in the Table 2 with a ratio of micropore of 44 and 62 % for OPAC and OPACS respectively.

Results of BET are shown in Table 2. As expected, the external surface, the pore size and the microporous volume are clearly favored after steam physical activation. We can conclude that steam activation produces activated carbons with a pronounced development of microporosity at the expense of mesoporosity as stated in other research works found in the literature [31].

The BET surface area of OPAC and CHAC were respectively 345 and 1227 m^2g^{-1} and the total pore volume and micropore volume were 0.240 cm^3g^{-1} and 0.106 cm^3g^{-1} (44 % of total volume), respectively, for OPAC and 0.542 cm^3g^{-1}. and 0.380 cm^3g^{-1} (70.1 % of total volume) for CHAC. The treatment with sulfuric acid has a significant impact on the porous structure, notably by increasing the specific surface area of 44 and 12.4 % for OPACS and CHACS respectively. These observed phenomena could be due to impurities found in activated carbon before sulfonization and which can block some of the pores [32], the sulfuric acid will play the role of a cleaner that eliminates the impurities and opens pores clogged by tar.

Nevertheless, the volume of micropores of CHAC decreased after treatment with H_2SO_4 to create other mesoporous volumes. Increasing the surface and creating a mesoporous volume can be attributed to the generation of gases from the reaction between the acid and the materials on the surface of the carbon, which reopens the closed micropores and creates new mesopores

374 [33]. However, micropores volume has increased with OPAC at the expense of mesopores. For
375 instance, micropores occupied 44 % of total porosity, after sulfonation, OPACS micropores
376 represent 61.8 % of total pores volume, while it decreased from 70.1 % with CHAC to 35%
377 with CHACS.
378 Although its higher specific surface, CHAC has a lower fixation rate of sulfur, this is probably
379 due to the hydrophobicity of their surface that reduces surface wetting necessary for
380 impregnation. Indeed, several studies have demonstrated that the polar sites of all activated
381 carbon attract water molecules, with different percentages depending on the raw material and
382 the process of manufacturing activated carbon, which enhances the adsorption of hydrophilic
383 compounds in the micropores [34].

384 Another reason could be a disparity in ionic exchange capacity between OPAC and CHAC
385 which allows the former to fix more sulfonic acid on its surface [35].

386 *3.2.3. X-ray diffraction analysis (XRD):*

387 The XRD pattern for the activated carbon and sulfonated activated carbon are illustrated in
388 Fig 3. The diffractogram recorded that all carbonaceous materials have shown two peaks
389 located at 2θ = 22.5 ° and 44 °, respectively, corresponding to the diffraction by graphite planes
390 of index (002) and (100), respectively.

391 The results show that the broad diffraction peak (2θ = 10-25º) can be attributed to the
392 amorphous structure as a major constituent of both AC. The weak and broad diffraction peak
393 (2θ = 40-50º) is due to the a-axis of the graphite structure [35].

394 The intensity of the base line I_{am} of the diffractogram is mainly related to the presence of non-
395 aromatic amorphous carbon in char [36].

The peak (100) is attributed to graphite structures in the plane [37]and reflects the size of the aromatic strata [38]. More the peak is narrower, the degree of condensation of the aromatic rings is high.

The peak (002) is attributed to the inter-reticular distance between the graphitic planes of the crystallites present in the char [339]. Theoretically, this peak is symmetrical. However, several studies have shown that an asymmetry characterized by the appearance of a shoulder on the left side of the peak (called the γ band) can reflect the presence of a stack of saturated structures such as aliphatic chains [40]. The region between 8 and 35 ° is therefore composed of two peaks (002) and γ band.

Diffractograms of sulfonated AC consist of two peaks corresponding to graphite planes (002) and (100). Suggesting that the chemical process does not affect the internal structure of carbon materials, this is consistent with many other reports, independently of the nature of the carbon used [41]. However, diffractograms of sulfonated AC show slight differences in the shapes and intensities of peaks:

- A shift of baseline signal indicating a drop in non-aromatic amorphous carbon concentration.

- Peak (100) became narrower after sulfonization revealing an increase in the condensation degree of aromatic cycles,

- Peak (002) became more symmetrical unveiling a decrease in the aliphatic carbon content.

Therefore, activated carbon becomes more aromatic under the effect of the sulfonation. The aliphatic carbon content (characterized by the γ band) has decreased because these structures weakly bound to the crystallites of char are removed as volatile compounds during the treatment with sulfuric acid. The treatment with H_2SO_4 has caused a tightening of the peak (002) which also results in a decrease in the inter-reticular distance d002 or a higher crystallite

size. This evolution reflects the rise of carbon structure order and is in agreement with the literature data [42].

3.2.4. Fourier Transform Infrared Spectroscopy (FT-IR):

The chemical nature of surface functionalities of OPAC, OPACS, CHAC and CHACS were investigated using FTIR analysis. Spectra of different samples are shown in Fig 4.

The most important absorption bands at frequency values were: OH stretching in hydroxyl groups (between 3135 cm^{-1} and 3445 cm^{-1}), C-O stretch vibration (196 and 1636 cm^{-1}), C-H deformation vibration (1384 cm^{-1}) and the specific spectral bands of sulfur are compatible with S=O and S-O stretching in sulfonic acid such as SO_3H and sulfates SO_4^{2-} [43]. The detection of the sulfonic acid is usually located in the wavenumber ranges 1080-1204 cm^{-1}. Whereas sulfates will appear between 833 and 458 cm^{-1}[43].

Changes in the relative intensity of bands, particularly for those located at around 1200 cm^{-1}, indicate a greater presence of the sulfonic acid in OPACS. These results support the results found in ultimate and proximate analysis, which explains the percentage of oxygen that increases due to the formation of the sulfonic acid.

3.2.5. Scanning Electron Microscopy (SEM):

Fig 5. presents SEM photographs of OPAC and CHAC before and after the sulfonation. Fig 5A and 5E show that OPAC and CHAC are composed of particles with varied morphologies and textures. OPAC particles are compact, differing with CHAC that are disorganized.

This is due to the anatomical orientation of the raw material, studies on the lignin distribution and the anatomical characteristics of the coconut and olive nut fibers were elaborated by Abdul K. *et al.* [44], These studies show that lignin is found in the cell walls of fibers, and that the olive nucleus has a much more compact structure without having phloems and meta-xylem.

which explains its compact morphology in fig (5A), in contrast to coconut, as phloems and meta-xylem, give it a more disordered structure.

Sulfonation has significantly modified char surface. Indeed, the OPACS has a mineral layer covering the vast majority of its surface (Fig 5B). This modification is very clear on the SEM images where mineral species appear brighter than the carbon matrix. While CHACS surface appears more orderly and more uniform. As mentioned before, capillary vessels, according to their functional botanical characteristics, leave voids in the structure of the raw material, which favors the development pores in the produced activated carbons.

Impregnation with H_2SO_4 takes advantage of the disordered, porous structure of the activated carbon to ensure rapid and uniform diffusion, which significantly reduces the presence of voids in the sulfonated activated carbon and gives it this uniform filamentous appearance [25]. This morphology is already observed in agricultural wastes treated with sulfuric acid [45].

SEM images of OPAC and OPACS fig (5C and 5D), show lots of changes in the morphology of the activated carbon as a result of sulfonation procedure. These changes consist mainly on the purification of activated carbon, by eliminating impurities such as tar stuck in the micropores, which gives the surface a more homogeneous appearance. This observation is in line with the increase of BET surface and mesoporosity of CHACS. The same aspect can be observed for CHAC and CHACS.

It is very important to note that the pore structure of activated carbon developed and modified during activation varies widely from one char to another and that pores of different shapes (cylindrical, conical or bottle-shaped) can be obtained. Bottle-like pores appear during pyrolysis. According to Gonzalez-Serrano E. et al. [46], during carbonization, there are certain minerals, that produce a plastic phase which facilitates its distribution in lignocellulosic materials and allows the generation of bottle-like pores [47]. Activation with H_2O vapor, allows

developing cone-shaped pores, generated by the gasification reactions of carbon, the pores have a conical shape due to the difference in H_2O concentration in the carbon grain and the difference in reactivity of the carbon atoms. Bottle shaped and cone-shaped pores can be seen clearly in figs (5C and 5H) [48].

3.3. Using sulfonated AC as catalyst for esterification

3.3.1. Turn Over Frequency of different catalysts

CHACS and OPACS were tested as catalysts for the methanolysis of FFA contained in olive pomace oil having an acidity of 126 mg_{KOH}/g_{oil}. Sulfuric acid was also used for comparison under conditions stated in authors research team's previous work [49]. The reaction advancement was followed with respect to time by analyzing the acidity of samples taken from the reactor each hour using different catalysts under different conditions

The results are presented in figure 6. As it can be noticed, two phases can be distinguished in the for different catalysts. A rapid phase where acid value (AV) decreases rapidly before arriving to a slow phase where the chemical equilibrium is approached. This observation is in line with those set by Stamenkovic et al. [50] who divided the kinetics of transesterification reaction following three consecutive phases. a mass transfer controlled one that is very short (few minutes) and can not be noticed at temperatures higher than 30°C with good agitation. Thus most studies deal with the reaction without taking it in account. While the chemically controlled phase can be divided into two pseudo-homogeneous parts. The first part is very fast while the second one, also called equilibrium phase is slow. The esterification process is very similar to transesterification due to the immiscibility of phases, the slow and the reversible character of the reaction and due to species entering in reaction. Thus the approach of Staminovic et al. could be representative of esterification also.

489 It can be noticed that the homogeneous catalysis has the highest conversion rate during the first
490 phase of reaction (t < 1h), while it has the lowest rate during the second one. The good
491 miscibility of sulfuric acid with other reagents gives a better performance at the beginning of
492 the reaction, but the accumulation of water started to slow down the reaction because of the
493 reverse reaction. Furthermore, the solubility of sulfuric acid in water leads to its dissociation
494 and deactivation. On the other hand, AC-based heterogeneous catalysts are hydrophobic which
495 allows them to absorb methanol and lipids and to repel water formed during reaction. Thus
496 reaction medium around SO_3H sites are more favorable for direct reaction than reverse one
497 which explains why these catalysts have steeper slopes at advanced stages of reaction.

498 OPACS and CHACS have similar trends during the first hour of reaction with higher FFA
499 conversion rates registered for CHACS. During the second period (t > 1h) the trends are shifted
500 and the OPACS results with fastest FFA conversion. The higher rate noticed with CHACS
501 during the first stage of reaction could be related to its higher surface area and mesoporous
502 volume (almost twice of those of OPACS) which allows a faster diffusion of reagents inside its
503 pores, especially that the mixture has a high viscosity at this phase. During the second phase (t
504 > 1 h) the highest content of SO_3H of OPACS leads to a better reaction rate despite its lower
505 surface area and mesoporous volume. In fact, with reaction advancement, more FFA are
506 transformed to methyl esters and the viscosity of the mixture becomes lower which reduces the
507 effect of mass transfer on reaction.

508 The trend of reaction with homogeneous and heterogeneous catalysts fits well with the
509 observations of Staminovic et al. with a very fast phase followed by a very slow one.
510 Concerning the fast phase, reaction using OPACS is significantly slower than those using
511 CHACS and Sulfuric acid as catalysts. In fact, the oil has lost 87% of its AV using
512 homogeneous catalyst during the first hour of reaction. The decrease in AV during the first
513 hour of reaction has also ranged between 72% (3:1, 10%) and 85.5% (9:1, 20%) when using

514 CHACS. While the use of OPACS resulted in a decrease of AV during the first hour ranging
515 between 61% (3:1, 10%) and 73.2% (9:1, 20%).

516 However, after 5 h of reaction OPACS and CHACS resulted on similar AV conversion ranging
517 between 75% and 99% with a slightly higher conversion for CHACS.

518 In order to analyze the performance of different catalysts, turn over frequency (TOF) was
519 compared for different catalysts under different conditions after 1h (TOF_{1h}) and 5 h (TOF_{5h}) of
520 reaction, respectively. Results are presented in Table 3. It can be clearly noticed that the
521 reaction is very fast during the first phase where the TOF_{1h} is on average 3.6 times and 4.2
522 times higher than TOF_{5h} for OPACS and CHACS respectively.

523 On the other hand, it is obvious that the CHACS has the highest efficiency per acid site,
524 followed by OPACS then by Sulfuric acid. When compared at same conditions, the TOF_{5h} of
525 CHACS is on average 3.15 times higher than that of OPACS. This ratio corresponds almost to
526 the ratio of sulfur content of OPACS divided by that of CHACS (3.133). That means that the
527 deficiency in acid sites was compensated by other aspects of the CHACS such as its mesopores
528 content that is twice that of OPACS. At the same time TOF_{1h} for CHACS is on average 3.7
529 times higher than that of CHACS which exceeds the ratio of sulfur contents. This observation
530 means that during the first phase the mass transfer through the pores of catalyst has a very
531 important role in the reaction.

532 TOF_{1h} and TOF_{5h} of OPACS are 2.6 - 4.6 times and 3 - 6 times higher than that of sulfuric acid,
533 respectively, at same methanol to FFA molar ratio. This can be explained by the
534 hydrophobicity of the activated carbon that repels water from reaction zone which enhances
535 reaction kinetics and preserves acid sites from dissociation. The highest TOF_{5h} of OPACS to
536 sulfuric acid ratio as compared to that of TOF_{1h} indicates that mass transfer in catalysts pores
537 has a higher effect during the first hour of reaction.

For both heterogeneous catalysts TOF_{1h} and TOF_{5h} are inversely proportional to catalyst loading. For instance, at constant molar ratio, increasing catalyst loading from 10% to 15% and to 20% divides TOF by almost 1.5 and 2 times respectively. These ratios are getting closer to 1.5 and 2 with the increase of molar ratio and reaction time. These trends reveal that increasing the catalyst loading does not bring lots of enhancement to the reaction output in terms of conversion. However, the stringent limit of 2 mg_{KOH}/g_{oil} makes the slight increase in conversion rates due to catalyst load increase meaningful.

At the same extent, increasing methanol to FFA ratio brings around 0.97% and 0.95% enhancement in TOF_{5h} per additional mole of methanol per mole of FFA for OPACS and CHACS respectively. This trend could be explained by the enhancement of reaction kinetics and the diffusion of reactive mixture inside catalyst pores due to lower viscosity.

3.3.2. Kinetic study

In order to shed lights on the second phase of reaction (t > 1 h) of reaction where it is meant to reach its equilibrium, it is suggested to lead a kinetic study. Among different models suggested in literature an irreversible, pseudo-first order kinetic model gave the best fit. Esterification reaction is presented in equation 8:

$$FFA + M \leftrightarrow ME + W \quad (8)$$

The rate of reaction can be then expressed as in equation 9

$$\frac{dFFA}{dt} = -k_1 FFA.M + k_2 ME.W \quad (9)$$

For an irreversible reaction k_2 is set to zero, while for a pseudo-first order reaction, the excess of alcohol is considered sufficiently high to consider that methanol concentration is constant during the reaction [51]. Thus equation 9 can be transformed to equation 10:

$$\frac{dFFA}{dt} = -k.FFA \quad (10)$$

Where $k = M_0.k_1$. With M_0 is the methanol concentration at the beginning of reaction. FFA in equation 10 can be replaced by acid value AV since $FFA = m_{oil}.AV/M_{KOH}$ where m_{oil} is the mass of oil used in the reaction and M_{KOH} is molar mass of KOH.

Using the integral method on the segment (t > 1 h) of the curve, .the rate constant of reaction was determined for all experiments led with all of three catalysts at different operating conditions. Results are presented in Table 4. Rate constants are higher when using OPACS with respect to CHACS and to homogeneous catalysts. At similar conditions k value when using OPACS is 1.11 to 1.85 times higher than that of CHACS which is lower than the ratio between sulfur (catalytic sites) contents of both catalysts. This means that the mass transfer through the pores and the hydrophobicity of catalysts are playing important roles. The mesopores of CHACS increase the mass transfer inside the catalyst and thus compensate the lower number of acid sites while its hydrophobicity repels formed water during reaction and enhances species balance around acid sites and approaches more the irreversible reaction model. Rate constants have increasing trends with the increase of alcohol:oil ratio and with catalyst loading and they vary in a linear way with both parameters. The increasing trend with catalyst loading is related to the increase in catalytic sites density. This trend was observed in different studies where increasing catalyst load increases activation energy and/or pre-exponential factor [52 - 54]. Increasing k with methanol loading is related to 2 aspects, the first one is obvious from equation 10 where $k = M_0.k_1$ while the second aspect is related to the decrease in mixtures viscosity which enhances mass transfer inside pores. In the case of CHACS, passing from a molar ratio of 3:1 to 6:1 and to 9:1 multiplies k by 2.3 times and 3.1 times on average, respectively. These values are 10 – 30% higher to what is expected by equation 10. In the case of OPACS, multiplying molar ratio by 2 and 3 times multiplies k by 1.6 times and 2.3 times on

584 average, respectively. These trends are 20-25% lower from what is expected based on
585 equation 10. These deviations from the suggested model could be related to the effects of mass
586 transfer of reagents through the pores of catalyst. Further investigations are needed in order to
587 take in consideration the mass transfer through the pores and it could not be covered in the
588 present work.

589 *3.3.3. Final product characterization*

590 At the highest loading of catalyst and methanol the acid value has reached 1.14 mg_{KOH}/g using
591 CHACS and 1.41 mg_{KOH}/g using OPACS. Although the highest rate during the second part of
592 reaction, CHACS exhibited a slightly highest FFA conversion rate, which emphasizes the
593 importance of the first phase of reaction. GC-FID analysis of the product obtained using
594 OPACS (9:1, 20%) has shown very low contents of mono, di, and triglycerides (0.4, 0.8 and 0
595 %) respectively with a viscosity of 3.02 mm^2/s at 40°C. At the same time, GC-MS has shown a
596 FAME content of 97.3%. Thus, it could be concluded that the used catalyst is able at the same
597 time to catalyze esterification and transesterification processes. A further optimization could be
598 needed in order to decrease FFA and diglycerides contents to meet EN14214 requirements
599 (0.5 mg_{KOH}/g and 0.2 % respectively) [55]. This would avoid a second step of reaction.

600 ## 4- Conclusions

601 In this study, solid acid catalyst was produced from olive pomace-based activated carbon by
602 sulfonation. Commercial activated carbon was also used for comparison. Catalysts were
603 characterized and used for the esterification of olive pomace oil (OPO).

604 Olive pomace was first pyrolyzed before undergoing an activation with superheated steam. The
605 resulting product is an activated carbon (OPAC) with a moderate specific surface dominated by
606 micropores. The sulfonation of OPAC increased the BET surface and the specific pore volume
607 by 80% and 36% respectively by cleaning pores from residual tar and by enlarging micropores.

608 This result was confirmed by XRD and SEM analysis. The final product was rather
609 microporous. Almost same results were obtained with commercial coconut husk based
610 activated carbon (CHAC) that was rather mesoporous.

611 Although its higher specific surface and porosity, CHAC fixed 70% less sulfur than OPAC.
612 This observation could be attributed to the lower hydrophobicity of the latter that allows a
613 better wetting of surfaces, leading to better impregnation of sulfur. FTIR spectroscopy has
614 shown that sulfur was mainly fixed in form of sulfonic acid in both catalysts, with lower peaks
615 corresponding to sulfates.

616 Esterification reaction was then performed using both catalysts and were compared to
617 homogeneous catalysis using sulfuric acid. Reaction order and rate constants were
618 determined under different operating conditions. Two phases of were distinguished. During
619 the first phase homogeneous catalysis is more efficient and FFA are converted faster.
620 During the second phase heterogeneous catalysts have a faster rate.

621 CHACS has a better performance during the first phase as compared to OPACS. While the
622 latter exhibits faster kinetics during second phase. Turn over frequencies (TOF) of different
623 catalysts were studied and after 5 h of reaction it turns out that both catalysts give similar
624 performances although the differences in acid sites densities and mesoporous volumes.
625 Increasing methanol to FFA molar ratio has increased TOF by almost 1% per mol of
626 methanol:mol FFA.

627 The second phase of reaction was modeled as a direct first order reaction. At different
628 conditions the suggested model gave a good fit. Some deviations were noticed concerning
629 the effect of methanol:FFA ration the rate constant evolution. Mass transfer through pores
630 could be responsible of this deviation. A more detailed mechanistic study could reveal its
631 exact effects.

The highest methanol and catalyst loading gave higher FFA conversion rates. When using 9:1 methanol:oil molar ratio and 20% catalyst load, both heterogeneous catalysts gave place to acid values lower than 2 mg_{KOH}/g. GC-FID/MS analysis of the one obtained using OPACS showed that its di-glycerides content is slightly higher than the requirements of EN14214, while mono and triglycerides respect them with a content of fatty acids methyl esters Higher than 97%. The viscosity was also measured and it recorded 3 mm^2/s.

References:

[1]. M. V. Lopez-ramon, C. Moreno-castilla, F. Carrasco-marın, and M. A. Alvarez-merino, "Chemical and physical activation of olive-mill waste water to produce activated carbons," vol. 39, pp. 1415–1420, 2001.

[2]. P. Vossen, "Olive Oil : History , Production , and Characteristics of the World ' s Classic Oils," vol. 42, no. 5, pp. 1093–1100, 2007.

[3]. J. C. Jose Antonio Alburquerque, J Gonzálvez, Dumeivy Garcia, "Agrochemical characterisation of 'Alperujo', a solid by-product of the two-phase centrifugation method for olive oil extraction," Bioresource Technology, pp. 195–200, 2004.

[4]. B. Leblon et al., SUSTAINABLE DEVELOPMENT – AUTHORITATIVE AND LEADING EDGE CONTENT FOR ENVIRONMENTAL Edited by Sime Curkovic. 2012.

[5]. M.-G. J. Jauhiainen, J.A. Conesa, R. Font, "Kinetics of the pyrolysis and combustion of olive oil solid waste," jornal of analytical and appleid pyrolysis, 2004.

[6]. C. Russo et al., "Product environmental footprint in the olive oil sector : State of the art," Environmental Engineering and Management Journ, . Vol.15, No. 9, 2019-2027 .

[7]. F. Cheng and X. Li, "Preparation and Application of Biochar-Based Catalysts for Biofuel Production," no. 1, pp. 1–35, 2018.

[8]. J. R. Kastner, J. Miller, D. P. Geller, J. Locklin, L. H. Keith, and T. Johnson, "Catalytic esterification of fatty acids using solid acid catalysts generated from biochar and activated carbon," Catalysis Today, vol. 190, no. 1, pp. 122–132, 2012.

[9]. T. Liu, Z. Li, W. Li, C. Shi, and Y. Wang, "Preparation and characterization of biomass carbon-based solid acid catalyst for the esterification of oleic acid with methanol," Bioresource Technology, vol. 133, pp. 618–621, 2013.

[10]. S. Dora, T. Bhaskar, R. Singh, D. V. Naik, and D. K. Adhikari, "Effective catalytic conversion of cellulose into high yields of methyl glucosides over sulfonated carbon based catalyst," Bioresource Technology, vol. 120, pp. 318–321, 2012.

[11]. M. Dehkhoda, A. H. West, and N. Ellis, " Biochar based solid acid catalyst for biodiesel production," "Applied Catalysis A, General," vol. 382, no. 2, pp. 197–204, 2010.

[12]. ASTM D3175-20, Standard Test Method for Volatile Matter in the Analysis Sample of Coal and Coke, ASTM International, West Conshohocken, PA, 2020

[13]. F. Kifani-sahban, L. Belkbir, and A. Zoulalian, " Study of the slow pyrolysis of Moroccan eucalyptus by thermal analysis," 1996, thermochimica acta.

[14]. ASTM D1102-84(2013), Standard Test Method for Ash in Wood, ASTM International, West Conshohocken, PA, 2013

[15]. ASTM D3174-12(2018), Standard Test Method for Ash in the Analysis Sample of Coal and Coke from Coal, ASTM International, West Conshohocken, PA, 2018

[16]. ASTM D664-18e2, Standard Test Method for Acid Number of Petroleum Products by Potentiometric Titration, ASTM International, West Conshohocken, PA, 2018A

[17]. Naoko Ellis, Feng Guan, Tim Chen, Conrad Poon, Monitoring biodiesel production (transesterification) using in situ viscometer, Chemical Engineering Journal 138 (2008) 200–206.

[18]. Ayhan Demirbad, Relationships derived from physical properties of vegetable oil and biodiesel fuels, Fuel 87 (2008) 1743–1748

682 [19].): EN ISO 3104 (1994) Petroleum products — Transparent and opaque liquids —
683 Determination of kinematic viscosity and calculation of dynamic viscosity, PR NF EN ISO
684 3104
685 [20]. G. Leofanti, M. Padovan, G. Tozzola, B. Venturelli, Surface area and pore texture of
686 catalysts, Catal. Today. 41 (1998) 207–219. doi:10.1016/S0920-5861(98)00050-9.
687 [21]. K.S.W. Sing, D.H. Everett, R.a.W. Haul, L. Moscou, R.a. Pierotti, J. Rouquerol,
688 T.Siemieniewska, International union of pure commission on colloid and surface chemistry
689 including catalysis* Reporting physisorption data for gas/solid systems with special reference to
690 the determination of surface area and porosity, Pure Appl. Chem. 54 (1982) 2201-2218.
691 [22]. L. A. De Macedo, "Torréfaction de biomasse lignocellulosique : effet catalytique du
692 potassium sur les espèces condensables Université de Lorraine, 2018.
693 [23]. S. Zellagui, "Pyrolyse et combustion de solides pulvérisés sous forts gradients
694 thermiques : Caractérisation de la dévolatilisation , des matières particulaires générées et
695 modélisation " université haute-alsace, 2017.
696 [24]. U. Arena, "Process and technological aspects of municipal solid waste gasification . A
697 review," Waste Management, vol. 32, no. 4, pp. 625–639, 2012.
698 [25]. M. J. Prauchner and F. Rodríguez-reinoso, "Chemical versus physical activation of
699 coconut shell : A comparative study," Microporous and Mesoporous Materials, vol. 152, pp.
700 163–171, 2012.
701 [26]. L. Medouni-haroune, F. Zaidi, S. Medouni-adrar, and M. Kecha, "Olive pomace: from
702 an olive mill waste to a resource, an overview of the new treatments" Journal of Critical
703 Reviews, vol. 5, no. 6, pp. 1–6, 2018.
704 [27]. V. Skoulou and A. Zabaniotou, "Investigation of agricultural and animal wastes in
705 Greece and their allocation to potential application for energy production," Renewable and
706 Sustainable Energy Reviews, no. January 2018, 2007.
707 [28]. R. Zanzi, K. Sjostrom, and E. Bjornbom, "Rapid pyrolysis of agricultural residues at
708 high temperature," Biomass and Bioenergy, vol. 23, pp. 357–366, 2002.

709 [29]. P. Fu et al., “Structural evolution of maize stalk / char particles during pyrolysis,”
710 Bioresource Technology, vol. 100, no. 20, pp. 4877–4883, 2009.
711 [30]. V. E. Diyuk, R. T. Mariychuk, and V. V Lisnyak, “Functionalization of activated
712 carbon surface with sulfonated styrene as a facile route for solid acids preparation,” Materials
713 Chemistry and Physics, vol. 184, pp. 138–145, 2016.
714 [31]. M. N. Alaya, M. A. Hourieh, A. M. Youssef, and F. E. F. Science, “Adsorption
715 Properties of Activated Carbons Prepared from Olive Stones,” Adsorption Science and
716 Technology, vol. 1, no. 1, pp. 27–42, 1999.
717 [32]. Kumar and H. M. Jena, “High surface area microporous activated carbons prepared
718 from Fox nut (Euryale ferox) shell by zinc chloride activation,” Applied Surface Science, vol.
719 356, pp. 753–761, 2015.
720 [33]. L. Tang, L. Li, R. Chen, C. Wang, W. Ma, and X. Ma, “Adsorption of acetone and
721 isopropanol on organic acid modi fi ed activated carbons,” Biochemical Pharmacology, vol. 4,
722 no. 2, pp. 2045–2051, 2016.
723 [34]. D. D. Do, S. Junpirom, and H. D. Do, “A new adsorption – desorption model for water
724 adsorption in activated carbon,” Carbon, vol. 47, no. 6, pp. 1466–1473, 2009.
725 [35]. S. Suganuma, K. Nakajima, M. Kitano, and D. Yamaguchi, “Hydrolysis of Cellulose by
726 Amorphous Carbon Bearing SO3H , COOH , and OH Groups,” Journal of the American
727 Chemical Society, pp. 12787–12793, 2008.
728 [36]. P. Fu, W. Yi, X. Bai, Z. Li, S. Hu, and J. Xiang, “ Effect of temperature on gas
729 composition and char structural features of pyrolyzed agricultural residues,” Bioresource
730 Technology, vol. 102, no. 17, pp. 8211–8219, 2011.
731 [37]. M. Guerrero, M. P. Ruiz, Á. Millera, M. U. Alzueta, and R. Bilbao, “Characterization of
732 Biomass Chars Formed under Different Devolatilization Conditions : Differences between Rice
733 Husk and Eucalyptus,” Energy & Fuels, no. 17, pp. 1275–1284, 2008.
734 [38]. M. Shahed et al., “Production , characterization and reactivity studies of chars produced
735 by the isothermal pyrolysis of flax straw,” Biomass and Bioenergy, vol. 37, pp. 97–105, 2011.

736 [39]. P. Lahijani, Z. Alimuddin, A. Rahman, and M. Mohammadi, “CO2 gasification
737 reactivity of biomass char : Catalytic influence of alkali , alkaline earth and transition metal
738 salts,” Bioresource Technology, vol. 144, pp. 288–295, 2013.
739 [40]. L. Lu, C. Kong, V. Sahajwalla, and D. Harris, “Char structural ordering during
740 pyrolysis and combustion and its in ¯ uence on char reactivity q,” FUEL, vol. 81, pp. 1215–
741 1225, 2002.
742 [41]. D. Vamvuka, S. Troulinos, and E. Kastanaki, “The effect of mineral matter on the
743 physical and chemical activation of low rank coal and biomass materials,” FUEL, vol. 85, pp.
744 1763–1771, 2006.
745 [42]. B. Manoj and A. G. Kunjomana, “Study of Stacking Structure of Amorphous Carbon by
746 X-Ray Diffraction Technique,” International Journal of electrochemical science, vol. 7, pp.
747 3127–3134, 2012.
748 [43]. R. Conley, “In Espectroscopia Infrarroja.,” 1979, vol. pp. 203-10.
749 [44]. Á. López-bernal, E. Alcántara, L. Testi, and F. J. Villalobos, “Spatial sap flow and
750 xylem anatomical characteristics in olive trees under different irrigation regimes,” Tree
751 Physiology, pp. 1536–1544, 2010.
752 [45]. Kula, M. Ug, C. Ali, and H. Karaog, “Adsorption of Cd (II) ions from aqueous
753 solutions using activated carbon prepared from olive stone by ZnCl 2 activation,” Bioresource
754 Technology, vol. 99, pp. 492–501, 2008.
755 [46]. J. J. Rodrı, “Development of Porosity upon Chemical Activation of Kraft Lignin with
756 ZnCl 2,” Ind. Eng. Chem. Res., pp. 4832–4838, 1997.
757 [47]. Harry Marsh Francisco Rodríguez Reinoso, “Activated Carbon”, Ed. Elsevier, Great
758 Britain, ISBN: 9780080444635. 2006.
759 [48]. C. E. De la Torre E., Guevara A., Revista Politécnica, EPN, 27-2, P.53. 2007.
760 [49]. S. Awad, M. Paraschiv, E. G. Varuvel, and M. Tazerout, “Bioresource Technology
761 Optimization of biodiesel production from animal fat residue in wastewater using response
762 surface methodology,” Bioresource Technology, vol. 129, pp. 315–320, 2013.

763 [50]. O.S. Stamenkovic, Z.B. Todorovic, M.L. Lazic, V.B. Veljkovic, D.U. Skala, Kinetics of
764 sunflower oil methanolysis at low temperatures, Bioresour. Technol. 98 (2007) 1131–1140.
765 [51]. Matthieu Tubino, José Geraldo Rocha Junior, Glauco Favilla Bauerfeldt, Biodiesel
766 synthesis with alkaline catalysts: A new refractometric monitoring and kinetic study, Fuel 125
767 (2014) 164–172
768 [52]. M. Berrios, J. Siles, M.A. Martìn , A. Martìn, A kinetic study of the esterification of
769 free fatty acids (FFA) in sunflower oil, Fuel 86 (2007) 2383–2388
770 [53]. Chia-Hung Su, Kinetic study of free fatty acid esterification reaction catalyzed by
771 recoverable and reusable hydrochloric acid, Bioresource Technology 130 (2013) 522–528
772 [54]. Thanh Lieu, Suzana Yusup, Muhammad Moniruzzaman, Kinetic study on microwave-
773 assisted esterification of free fatty acids derived from Ceiba pentandra Seed Oil, Bioresource
774 Technology 211 (2016) 248–256
775 [55]. Committee for Standardization Automotive fuels—fatty acid methyl esters (FAME) for
776 diesel engines—requirements and test methods. European Committee for Standardization,
777 Brussels; 2003a. Method EN 14214.

778

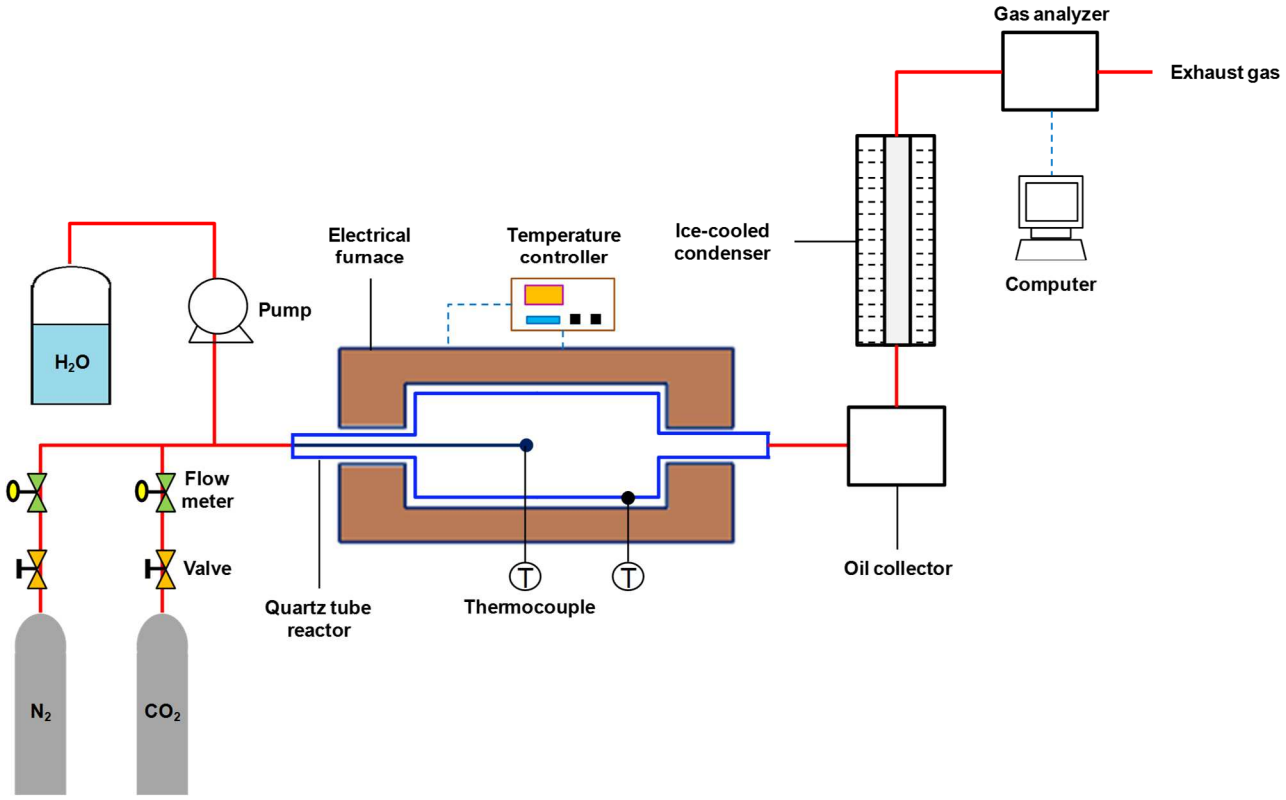

Fig. 1. Experimental set-up

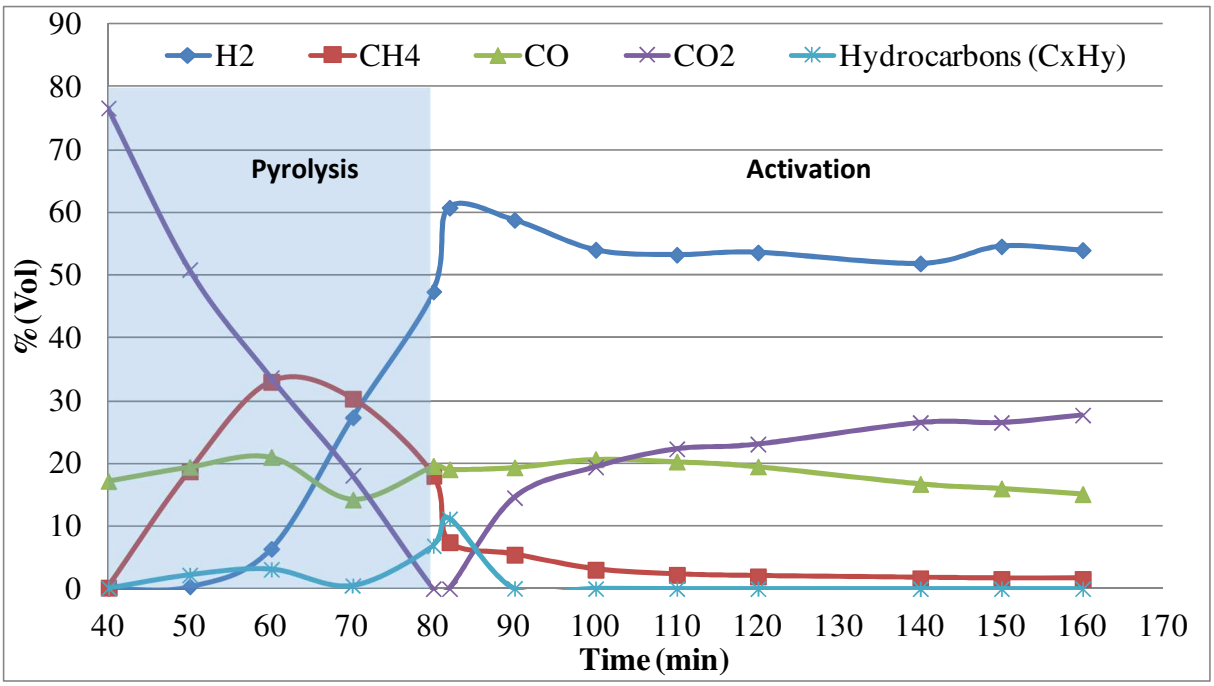

Fig. 2. Composition of gases produced during activation of olive pomace char

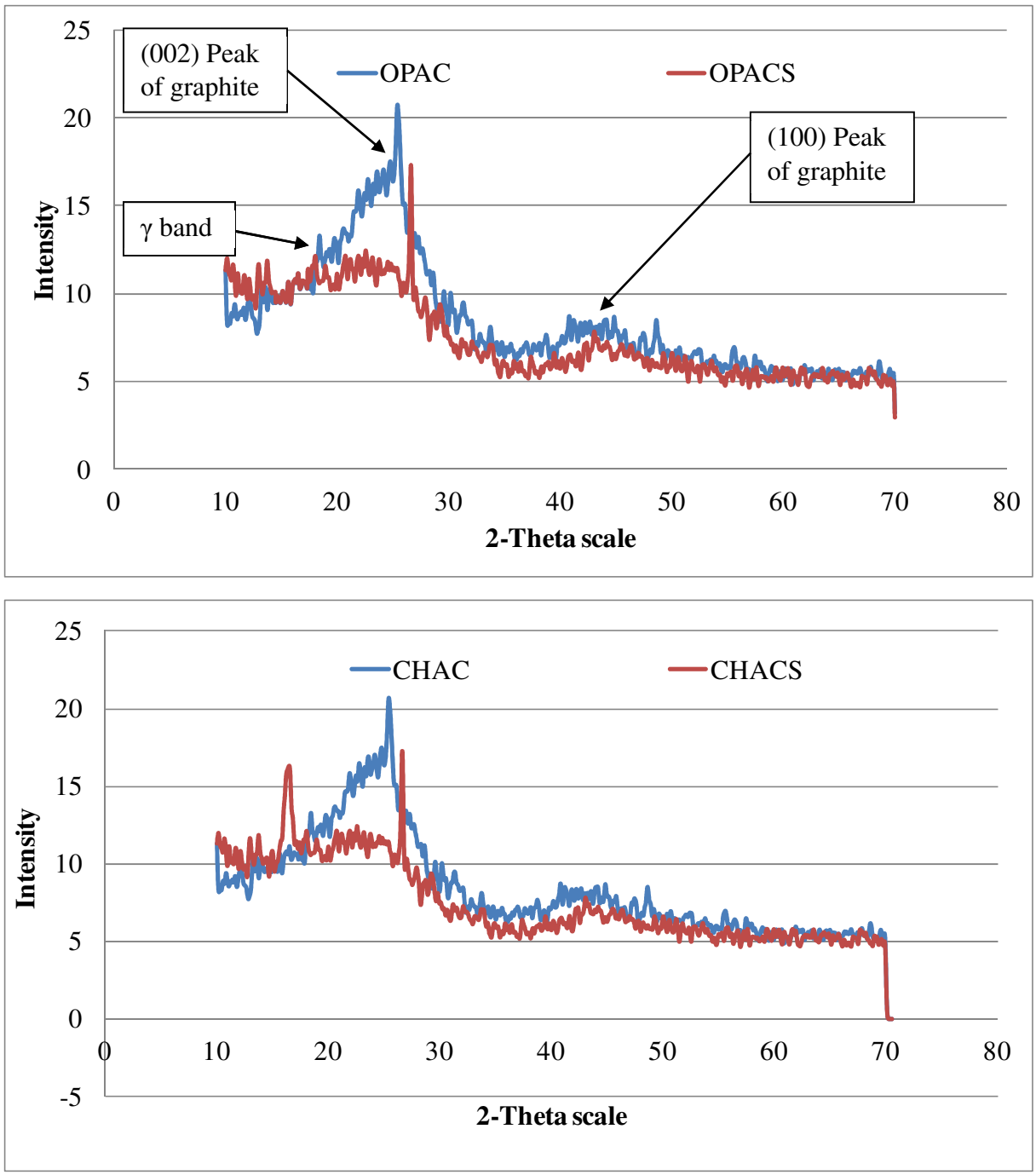

Fig. 3. Typical XRD patterns of the initial OPAC (olive pomace activated carbon), OPACS (sulfonated olive pomace activated carbon), CHAC (commercial coconut husk based activated carbon) and CHACS (sulfonated commercial coconut husk based activated carbon) samples

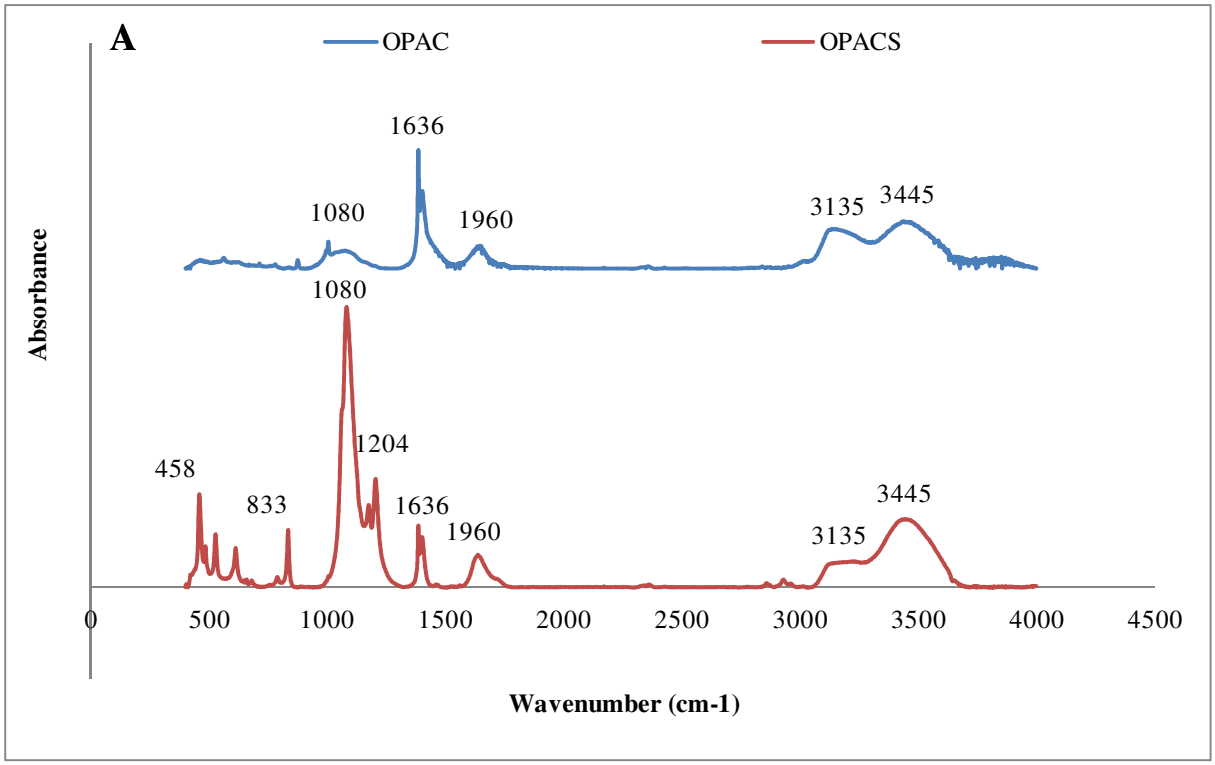

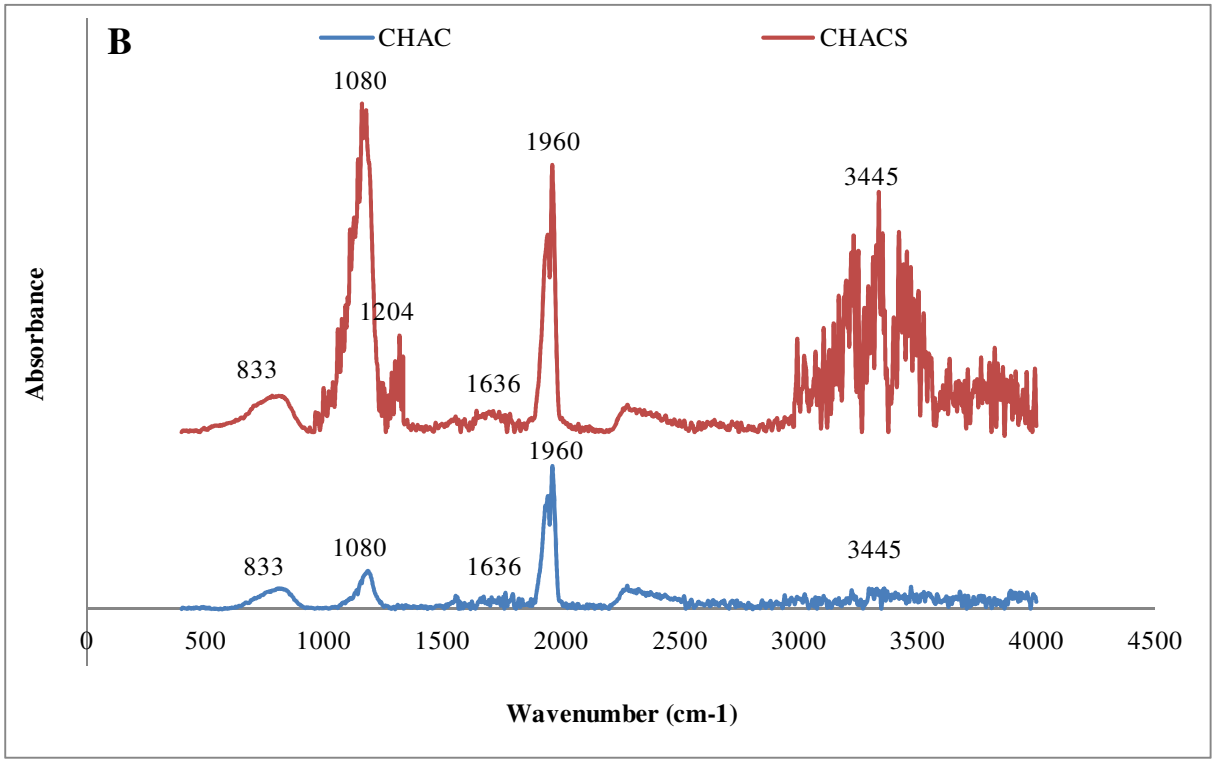

Fig. 4. Spectrum of FTIR analysis from (A): OPAC (olive pomace activated carbon) and OPACS (sulfonated olive pomace activated carbon) and (B): CHAC (commercial coconut husk based activated carbon) and CHACS (sulfonated commercial coconut husk based activated carbon)

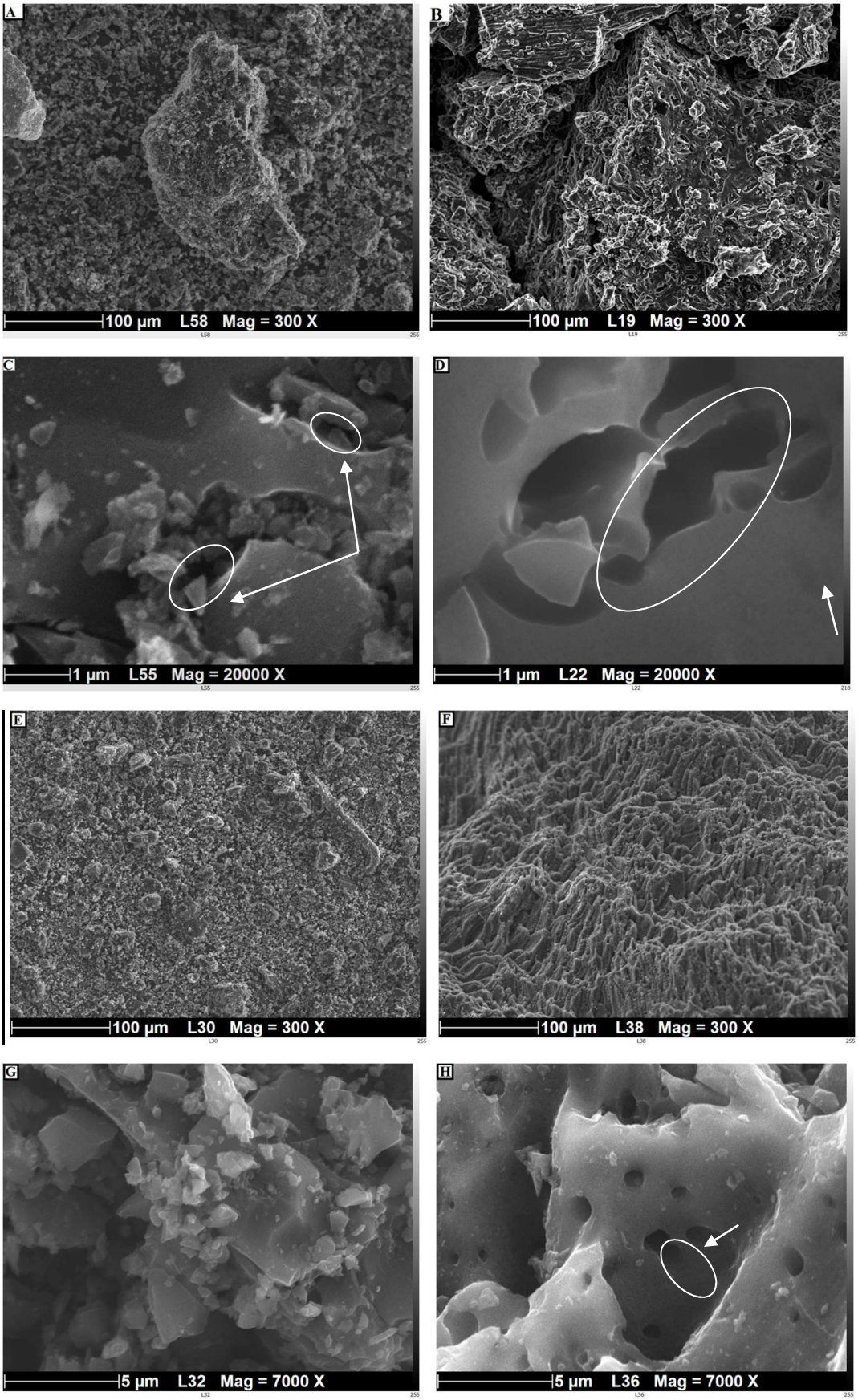

Fig. 5. SEM micrographs of (A and C) OPAC (olive pomace activated carbon), (B and D) OPACS (sulfonated olive pomace activated carbon), (E and G) CHAC (commercial coconut husk based

activated carbon) and (F and H) CHACS (sulfonated commercial coconut husk based activated carbon).

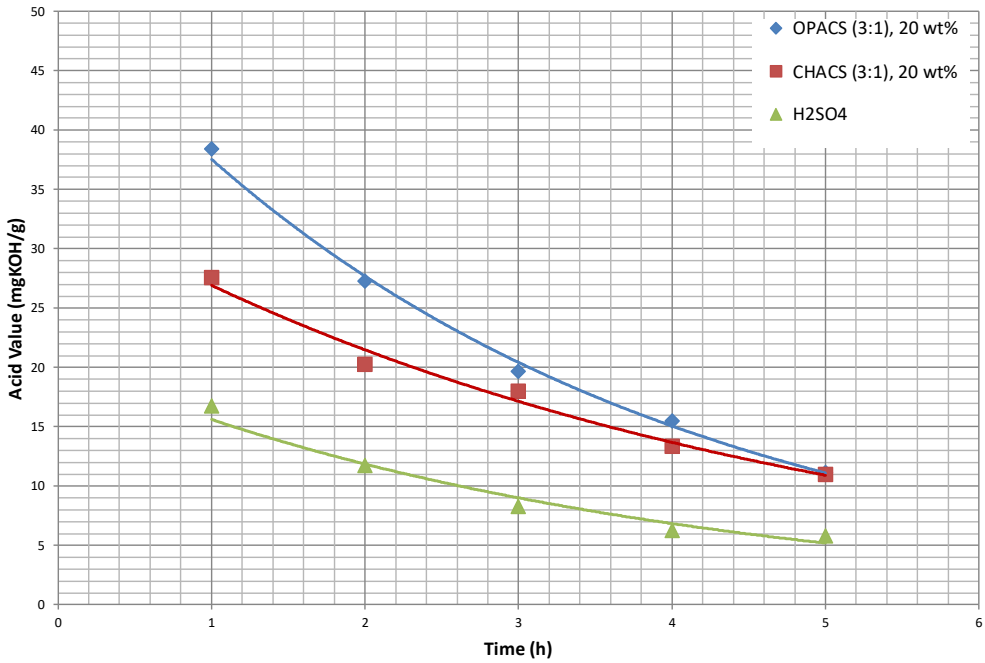

Fig. 6. Acid value evolution of oil using OPACS (sulfonated olive pomace activated carbon), CHACS (sulfonated commercial coconut husk based activated carbon) and Sulfuric acid using 3:1 methanol to FFA molar ratio

Table 1: Ultimate and Proximate Analysis

Biomass samples	*Ultimate Analysis (wt %)*					*Proximate Analysis*	
	% N	***% C***	***% H***	***% S***	***% O***	***Ash***	***Volatile's yield***
Olive pomace	0.82	45.31	5.54	LD	41.51	0.32	71.15
Bio-char	1.06	77.95	1.76	LD	4.41	7.88	
Sulfonated Bio-char	3.25	65.66	1.60	LD	7.38	8.45	
OPAC	0.43	85.14	0.86	LD	1.98	8.48	
OPACS	0.33	75.0	1.22	3.54	10.95	8.95	
CHAC	LD	90.05	0.38	LD	1.52	7.99	
CHACS	LD	87.73	0.77	1.13	6.12	8.44	

Results expressed in% by mass

LD : lowest than the limit of detection ***(LD < 0,06 % on CHNS-O)***

OPAC*: Olive Pomace Activated Carbon*

OPACS: *Sulfonated Olive Pomace Activated Carbon*

CHAC: Coconut Husk Activated Carbon

CHACS: Sulfonated Coconut Husk Activated Carbon

Table 2: Physical characteristics of solid acid carbon catalysts

Samples	Surface area [a] (m^2/g)	Total pore volume [b] (cm^3/g)	Micropore [*b] Volume (cm^3/g)	Mesopore [*c] volume (cm^3/g)
OPAC	345.31 ± 4.91	0.240	0.106	0.125
OPACS	618.18 ± 9.18	0.328	0.203	0.074
CHAC	1227.01 ± 7.4646	0.542	0.380	0.001
CHACS	1379.91 ± 15.23	0.784	0.274	0.152

For Abbreviations please refer to table 1

***** Micro: Dp < 2 nm; Meso: 2 < Dp < 50 nm; Macro: Dp > 50 nm.

a: single point surface area at p/p° = 0.290836494 ; b: determined from t-plot model; c: determined from BJH adsorption pore distribution.

Table 3: TOF of esterification using OPACS, CHACS and sulfuric acid under different conditions

	OPACS			**CHACS**			**H_2SO_4**
Catalyst loading ►	**10%**	**15%**	**20%**	**10%**	**15%**	**20%**	**3.6%**
Methanol : oil molar ratio▼	**TOF_{1h} (h^{-1})/TOF_{5h} (h^{-1})**						
3 :1	12.452/3.455	8.273/2.386	7.069/1.854	46.393/10.897	32.582/7.478	24.632/5.815	2.692/0.595
6 :1	12.797/3.740	8.729/2.524	7.105/1.957	46.154/11.834	33.602/8.136	25.300/6.144	-
9 :1	13.754/3.932	9.727/2.638	7.442/2.011	50.544/12.329	34.070/8.282	27.231/6.314	-

For Abbreviations please refer to table 1

Table 4: Constant rate of esterification using OPACS, CHACS and sulfuric acid under different conditions

	OPACS			**CHACS**			**H_2SO_4**
Catalyst loading ►	**10%**	**15%**	**20%**	**10%**	**15%**	**20%**	**3.6%**
Methanol : oil molar ratio▼				**k (h^{-1})**			
3 :1	0.23598	0.294	0.304	0.143	0.158	0.207	0.275
6 :1	0.38111	0.432	0.522	0.332	0.390	0.437	-
9 :1	0.5681	0.604	0.784	0.445	0.502	0.668	-

For Abbreviations please refer to table 1